

## An enhanced sea-ice thermodynamic model applied to the Baltic Sea

Letizia Tedesco<sup>1)2)</sup>, Marcello Vichi<sup>1)3)</sup>, Jari Haapala<sup>4)</sup> and Tapani Stipa<sup>4)</sup>

<sup>1)</sup> *Centro Euro-Mediterraneo per i Cambiamenti Climatici (CMCC), Viale Aldo Moro 44, I-40127 Bologna, Italy*

<sup>2)</sup> *Centro Interdipartimentale di Ricerca per le Scienze Ambientali (CIRSA), University of Bologna, Via Tombesi dall'Ova 55, I-48100 Ravenna, Italy*

<sup>3)</sup> *Istituto Nazionale di Geofisica e Vulcanologia, Viale Aldo Moro 44, I-40127, Bologna, Italy*

<sup>4)</sup> *Finnish Institute of Marine Research, P.O. Box 2, FI-00561 Helsinki, Finland*

*Received 18 Oct. 2007, accepted 19 Aug. 2008 (Editor in charge of this article: Timo Huttula)*

Tedesco, L., Vichi, M., Haapala, J. & Stipa, T. 2009: An enhanced sea-ice thermodynamic model applied to the Baltic Sea. *Boreal Env. Res.* 14: 68–80.

A refined Semtner 0-layer sea-ice model (ESIM1) is presented and applied to the Baltic landfast sea ice. The physical model is capable of simulating seasonal changes of snow and ice thickness. Particular attention is paid to reproducing the snow-ice and the superimposed-ice formation which play important roles in the total mass balance of the Baltic sea-ice. The model prognostic variables include all kinds of ice and snow layers that may be present during a Baltic landfast ice season and, in general, in every coastal area of an ice-covered ocean. The assessment of the model capabilities was done for 1979–1993 for four different stations in the Baltic Sea. A sensitivity test stresses the relevant role of some of the physical parameters, such as the oceanic heat flux, while a scenario analysis highlights the robustness of the model to perturbed physical forcing. Our results show that one of the key variables in modelling sea-ice thermodynamics is the snow layer and its metamorphism, and including the meteoric ice dynamics into a sea-ice model is relevant to properly simulate any ice season, also in view of climate change scenarios.

### Introduction

Though sea ice is only a very thin layer between the ocean and the atmosphere, it plays an important role in the Earth's climate system. The high albedo and its positive feedback, the strong insulating effect, the physical barrier it creates between the atmosphere and the ocean, and its impact on the large-scale thermo-haline structure of water masses make sea ice an active component of the climate system. It is, thus, likely that sea ice acts as a very sensitive indicator of a global climate change (Eicken 2003).

The evolution of the pack ice is driven by heat, radiation and momentum exchanges between the ocean and the atmosphere, which can be decomposed in thermodynamic (thermal growth/decay) and dynamic processes (drift, lead openings, ridging). In the coastal fast-ice regions, sea-ice evolution is determined fully by thermodynamic processes. These regions are indeed spatially limited, but are key factors that affect the functioning of high latitude ecosystems.

The first attempt to study sea-ice thermodynamics was the development of an analyti-

cal model by Stefan (1891). Later, Untersteiner (1964) and Maykut and Untersteiner (1971) moved to rather complex numerical modelling and Semtner (1976) simplified their model for numerical investigation of climate. Leppäranta (1983) introduced also snow compaction and snow-ice formation in his numerical simulations. Cox and Weeks (1988) began to study the thermal role of brines. Later Cheng *et al.* (2006) modelled the superimposed-ice formation during melting periods. During the last decades other variations of such numerical models were developed, with different complexity which aimed at different applications from the smallest to the largest temporal and spatial scales. However, not much effort has been put into analysing the properties of sea-ice thermodynamic modelling from a biogeochemical perspective and in regions where biomass production may have significant impacts on the global carbon cycle

Temperature, salinity, space, nutrients and light availability are the main environmental factors that affect the growth, distribution and abundance of sea-ice algae. At the bottom of the ice sheet, temperature, salinity, space and nutrients are more favourable to sea-ice algae growth, but primary production is often limited by thick snow covers that prevent a sufficient penetration of light. The situation is opposite on top of the ice sheet. Snow ice and superimposed ice play important roles, not only because they change the snow properties and the consequent rates of ice growth, but also because they create suitable habitats for sea-ice algae, bringing nutrients — by flooding events and melt-refreeze cycles — where the light is more available.

In this paper, we present a Semtner 0-layer model refined in a very comprehensive — in terms of a number of physical processes that have been included — thermodynamic sea-ice model. The Baltic Sea is characterized by rather complex melt-freeze cycles and more snow-ice formation than any other sea, which leads to the necessity of including the superimposed-ice and snow-ice layers to compute the total ice/snow mass balance. The stratification beneath the ice tends to be stable in the Baltic Sea and the oceanic heat flux remains generally small. The flux can thus be assumed constant allowing to compute only one sea-ice layer.

In our case, the aim of this model is the coupling with a biogeochemical flux model (BFM, Vichi *et al.* 2007a, 2007b). Therefore, the chosen physical processes have been included having in mind the description of the habitat for biogeochemical developments. The results have been compared with observations at four different stations. We further analysed the sensitivity of the model to some of the physical parameters, such as the albedo and the oceanic heat flux and to the new addition of relevant physical processes. Finally, we assessed the robustness to changes in the physical forcings.

## Description of the physical model

Following Semtner 0-layer model (Semtner 1976, hereafter referred to as S0), the sea-ice system consists of one layer of ice and one layer of snow on top. The model is developed in such a way that, depending on the required complexity, more layers of sea ice can be added and simulated. Differently from S0, prognostic variables include two layers of snow (two density classes), three layers of ice (superimposed ice, snow ice and sea ice), and temperature at the surface and in each layer. Sea ice stays isosaline with  $S = 5‰$ . The numerical step is 1.5 hours (*see* Fig. 1 for a schematic drawing of the model and Table 1 for the values of the model parameters). In all the following equations the subscript ‘s’ indicates snow, ‘i’ ice, ‘sn’ snow ice, ‘ss’ superimposed ice, ‘mi’ meteoric ice, ‘si’ sea ice and ‘w’ seawater. The MATLAB code of the model is freely available for download at the BFM website (<http://www.bfm.cmcc.it/>).

As in S0, a 1-dimensional heat conduction equation governs the vertical heat fluxes, defined positive downwards, at the boundaries and among different layers. Unlike S0, when sea ice is the only layer of the ice sheet, the sea-ice temperature equation also embeds the presence of the penetrating solar radiation which depends on the albedo  $\alpha$  and on the extinction coefficient  $\kappa$ :

$$(\rho c)_{s,i} \frac{\partial T_{s,i}(z,t)}{\partial t} = \frac{\partial}{\partial z} \left( k_{s,i} \frac{\partial T_{s,i}(z,t)}{\partial z} \right) + (1 - \alpha_{s,i}) F_s e^{-\kappa_i z} \quad (1)$$

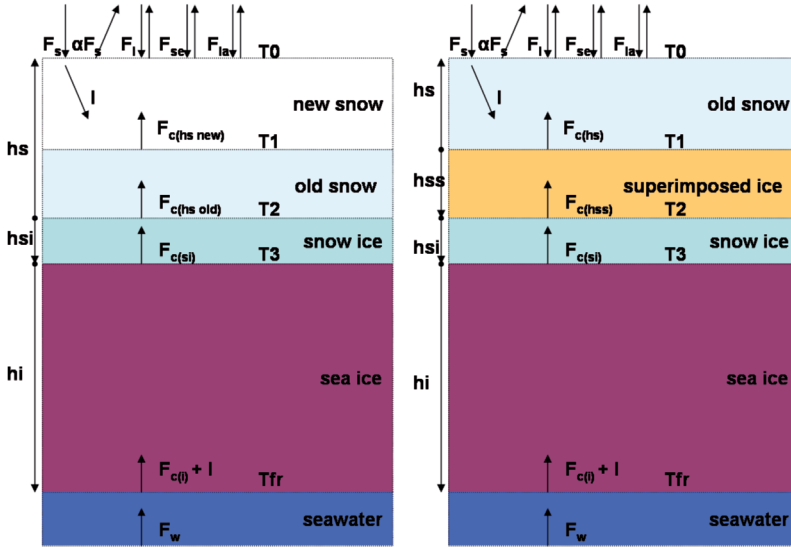


**Fig. 1.** General structure of the ESIM1 (heat fluxes, temperatures, snow and ice layers) during growth (left) and melting (right) periods.

where  $\rho$  is the density,  $c$  is the heat capacity,  $T$  is the temperature,  $k$  is the thermal conductivity and  $F_s$  is the incoming solar radiation.

The different layers are supposed to be in thermal equilibrium and the temperatures at the interfaces are derived from the continuity of the

heat fluxes (Fig. 1). The surface temperature is obtained by linearly approximating the surface fluxes, expanding in a Taylor series and iterating according to the Newton-Raphson method for 20 times with a convergence criterion of 0.01 K. Surface, snow, snow-ice, superimposed-ice and

**Table 1.** The ESIM1 parameters.

Parameter	Value	Unit	Source
Density of air $\rho_a$	1.225	kg m <sup>-3</sup>	
Density of new snow ( $\rho_{wy}$ )	200	kg m <sup>-3</sup>	
Density of snow $\rho_s$	400	kg m <sup>-3</sup>	
Density of snow ice $\rho_{sn}$	880	kg m <sup>-3</sup>	
Density of superimposed ice $\rho_{ss}$	850	kg m <sup>-3</sup>	
Density of sea ice $\rho_{si}$	900	kg m <sup>-3</sup>	
Density of seawater $\rho_w$	1026	kg m <sup>-3</sup>	
Thermal conductivity of new snow $k_{sy}$	0.056	W m <sup>-1</sup> K <sup>-1</sup>	
Thermal conductivity of snow $k_s$	0.180	W m <sup>-1</sup> K <sup>-1</sup>	
Thermal conductivity of snow ice $k_{sn}$	0.950	W m <sup>-1</sup> K <sup>-1</sup>	
Thermal conductivity of superimposed ice $k_{ss}$	0.900	W m <sup>-1</sup> K <sup>-1</sup>	
Thermal conductivity of sea ice $k_{si}$	2.000	W m <sup>-1</sup> K <sup>-1</sup>	
Extinction coefficient of sea ice $\kappa_{si}$	1.5–17.1	m <sup>-1</sup>	Maykut and Untersteiner 1971
Heat capacity of sea ice $c_{si}$	2 093	J kg <sup>-1</sup> K <sup>-1</sup>	
Heat capacity of snow ice $c_{sn}$	2 093	J kg <sup>-1</sup> K <sup>-1</sup>	
Heat capacity of superimposed ice $c_{ss}$	2 093	J kg <sup>-1</sup> K <sup>-1</sup>	
Heat capacity of snow $c_s$	2 093	J kg <sup>-1</sup> K <sup>-1</sup>	
Specific heat of air $c_a$	1 004	J kg <sup>-1</sup> K <sup>-1</sup>	
Specific heat of seawater $c_w$	4 186	J kg <sup>-1</sup> K <sup>-1</sup>	
Surface albedo of snow $\alpha_s$	0.750		Flato and Brown 1996
Surface albedo of snow/superimposed ice $\alpha_{sn,ss}$	0.56–0.7		Perovich 1996
Surface albedo of sea ice $\alpha_{si}$	(f of $h_i, h_s$ )		Flato and Brown 1996
Surface albedo of seawater $\alpha_w$	0.06		Perovich 1996

sea-ice temperatures are computed by solving a tridiagonal matrix of the heat conduction equation in each layer.

The snow compaction, snow-ice and superimposed-ice formation are fast processes and the thicknesses are assumed to reach an instantaneous equilibrium. The model is structured in such a way that, when snow compaction, snow-ice and superimposed-ice formation are initiated, the snow and ice fractions are transformed instantaneously at the next time step, thus changing their properties, such as density, thermal conductivity, heat capacity and albedo (Table 1).

Snow accumulates on top of the surface layer whenever the air temperature is below the freezing point of snow (273.15 K) and an ice layer is already present. If young fallen snow ( $(h_s)_y$ ) accumulates on an already present snow layer, snow compaction initiates by specifying the following instantaneous equilibrium:

$$h_s = (h_s)_y \frac{(\rho_s)_y}{\rho_s}. \quad (2)$$

The total surface fluxes include shortwave ( $F_s$ ) and longwave radiation ( $F_l$ ), sensible ( $F_{se}$ ) and latent ( $F_{lr}$ ) heat (Fig. 1). At the surface, snow, snow-ice, superimposed-ice and sea-ice melt whenever the surface temperature is at the melting point and the rate of melting is determined by the net heat flux balance between the surface fluxes and the conductive fluxes. As in S0, if the surface heat fluxes exceed the conductive fluxes, the imbalance in the surface energy budget contributes to increase the conductive flux of the surface layer and the surface energy balance changes accordingly.

The temperature at the bottom of the ice sheet is set constant at the freezing point of seawater at the given salinity (272.88 K). The oceanic heat flux at the ice–water interface is represented by constant values depending on the model location (ranging between 0 and 9 W m<sup>-2</sup>). At the bottom, ice growth or melting is regulated by the net heat flux balance between the oceanic and conductive fluxes.

As originally proposed by Fichfet and Morales Maqueda (1999), if the ice draft exceeds the ice thickness, i.e.

$$\frac{h_s \rho_s - h_{sn} (\rho_w - \rho_{sn})}{(\rho_w - \rho_{si})} > h_{si}, \quad (3)$$

then snow-ice formation is initiated. Snow density and compaction are changed accordingly and a new isostatic equilibrium is prescribed. We currently assume no addition of seawater mass. Snow is compressed to an amount of new snow-ice equal to the initial depression below the water line, as originally in Schmidt *et al.* (2004):

$$h_{sn} = \frac{\rho_s h_s + (\rho_{si} - \rho_w) h_{si} + (\rho_{mi} - \rho_w) h_{mi}}{\rho_w - \rho_{mi} + \beta \rho_s}, \quad (4)$$

$$h_s = (h_s)_y - \beta \left( h_{sn} + \frac{(\rho_s)_y (h_s)_y}{\rho_w + \beta \rho_s - \rho_{mi}} \right), \quad (5)$$

where  $\beta$  is an empirical coefficient of conversion between snow ice and sea ice (after Leppäranta 1983). Snow ice melts according to the same energy balance previously described for snow and sea ice.

If melted snow re-freezes in contact with an ice layer, superimposed-ice formation begins by transforming a fraction of snow, depending on snow properties, in superimposed ice (Cheng *et al.* 2006):

$$h_{ss} = (h_s)_{melt} \frac{\rho_s}{\rho_{ss}}. \quad (6)$$

In order to properly simulate the onset and melting of sea ice, we coupled the Enhanced Sea Ice Model (ESIM1) to a simple ocean mixed-layer 10-m thick. During ice-free periods, the slab ocean computes an heat budget equation and resolves the mixed-layer temperature of this isothermal layer as

$$\rho_w c_w h_w \frac{\partial T_w(t)}{\partial t} = F_{tot}, \quad (7)$$

where  $h_w$  stands for the depth of the layer,  $T_w$  for its temperature and  $F_{tot}$  for the net heat flux at the surface.

## Experiment design and methods

Model performance, in terms of seasonal evolutions of snow, snow-ice, superimposed-ice and sea-ice thickness and inter-annual variability of the thermal growth of sea ice, were assessed by comparison with regular sea-ice observations. The model was implemented in the Baltic Sea at four different stations (Fig. 2):



**Fig. 2.** Location of the stations for model comparison with observations.

Ajos (65°39.8'N, 24°31.4'E), Kummelgrund (62°09.3'N, 21°09.5'E), Jussarö (59°53.4'N, 23°31.1'E) and Kotka (60°27.3'N, 26°57.2'E). Ajos is the northernmost station and it is characterized by the most severe winters, more ice formation, snow accumulation, snow-ice formation and faster melting with minor superimposed-ice growth. Jussarö is the southernmost station and it is characterized by less severe winter, less sea-ice growth and snow precipitation, though consistent superimposed ice grows during the melting period. Kummelgrund is latitudinally located between Ajos and Jussarö and has intermediate characteristics between the two. Kotka is the easternmost station and shows similar characteristics to Jussarö, but since it is located north of Jussarö the area is affected by higher sea-ice growth rate.

The meteorological data were taken from ECMWF ERA-15 6h Reanalysis data at 2.5 degrees resolution (Gibson *et al.* 1997) considering air temperature at 2-m height, total cloud cover, wind speed at 10-m height, large scale precipitation and convective precipitation. Due to biases in the ERA-15 database, we used NCEP 6h Reanalysis (Kalnay *et al.* 1996) for irradiance

and specific humidity at the surface and at 2 m height. The weekly observations of snow, snow-ice, superimposed-ice and sea-ice thicknesses were provided by the Ice Service at the Finnish Institute of Marine Research. The chosen simulation period was 1979–1993.

Assuming the normality in the distribution of the residuals of ice thickness, the best fit for every station was chosen with respect to the following criteria: mean, variance, linear correlation, centered-root-mean-square error, kurtosis and skewness indices.

Model sensitivity was tested by using an index  $S$ , which considers both the variation of the input parameter and the consequent changes of the output variables (Saltelli 2005), i.e.:

$$S = \frac{\frac{O^+ - O^-}{\sigma O}}{\frac{I^+ - I^-}{\bar{I}}}, \quad (8)$$

where  $\bar{I}$  represents the chosen parameter (for instance, albedo) and

$$I^+ = (1 + \gamma) \bar{I} \quad (9)$$

$$I^- = (1 - \gamma) \bar{I} \quad (10)$$

where  $\gamma = 0.1$ ,  $O^+$  and  $O^-$  are the outputs of the studied model variable (total ice thickness) corresponding to  $I^+$  and  $O^-$ , respectively, while  $\sigma O$  is the standard deviation of total ice thickness for the control simulation. When  $S$  is close to 0, the relative changes in the model output (with respect to the observed standard deviation) are smaller than changes in the value of the parameter. If, on the other hand,  $S$  is closer to 1, changes in the model output are larger than variations in the parameter, and the model is very sensitive.

We also analysed the sensitivity of the model to the new physical processes, such as the inclusion of meteoric ice dynamics. Finally, we tested the dependence on the NCEP and ERA-15 Reanalysis data resolution by perturbing 10% their value at every time step.

## Model results and comparison

ESIM1 was calibrated using albedo and oceanic

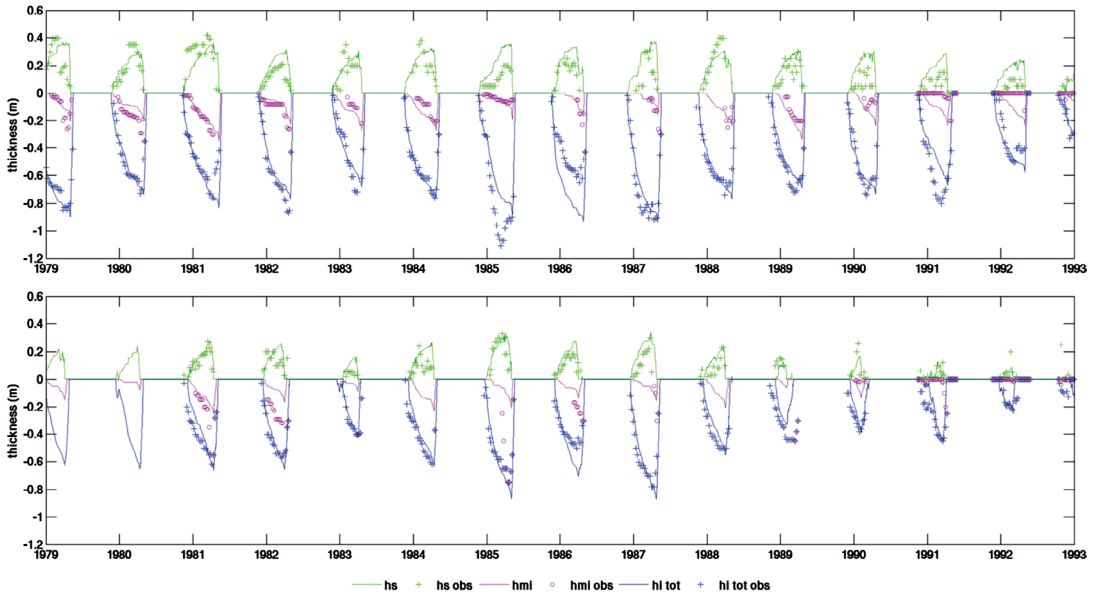


Fig. 3. Observations and model simulations at Ajos (above) and Kummelgrund (below) stations for 1979–1993. The two types of snow are grouped together ( $h_s$ ) and plotted in the positive ordinate. Snow ice and superimposed ice are also grouped together as an intermediate layer ( $h_m$ ) and plotted in the negative ordinate. The total ice thickness ( $h_{i\text{ tot}}$ ) is shown in the negative ordinate as the sum of the intermediate layer and the sea-ice thickness.

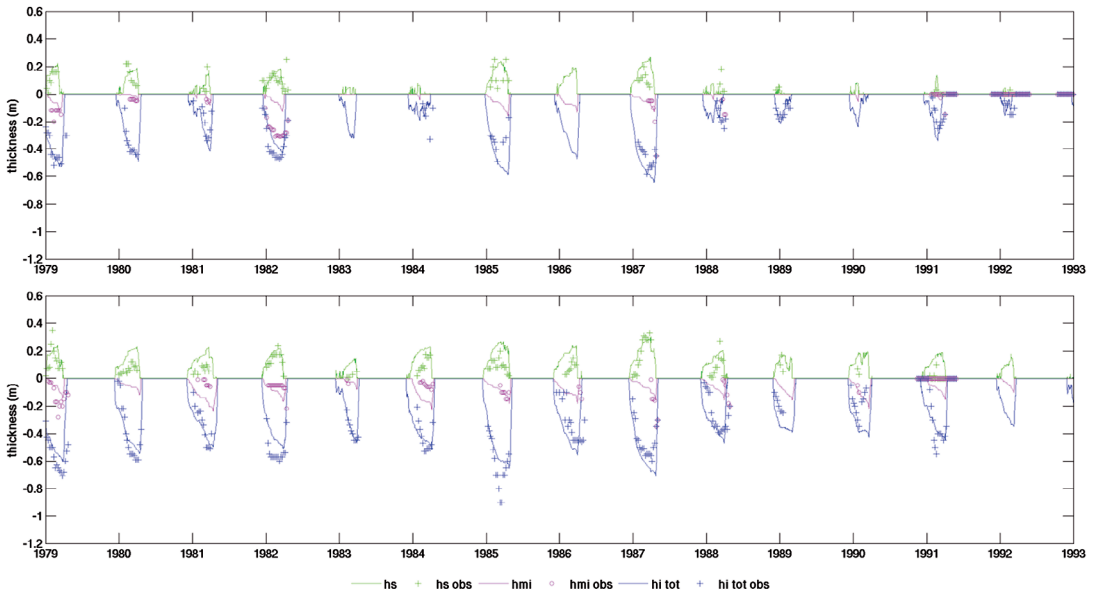
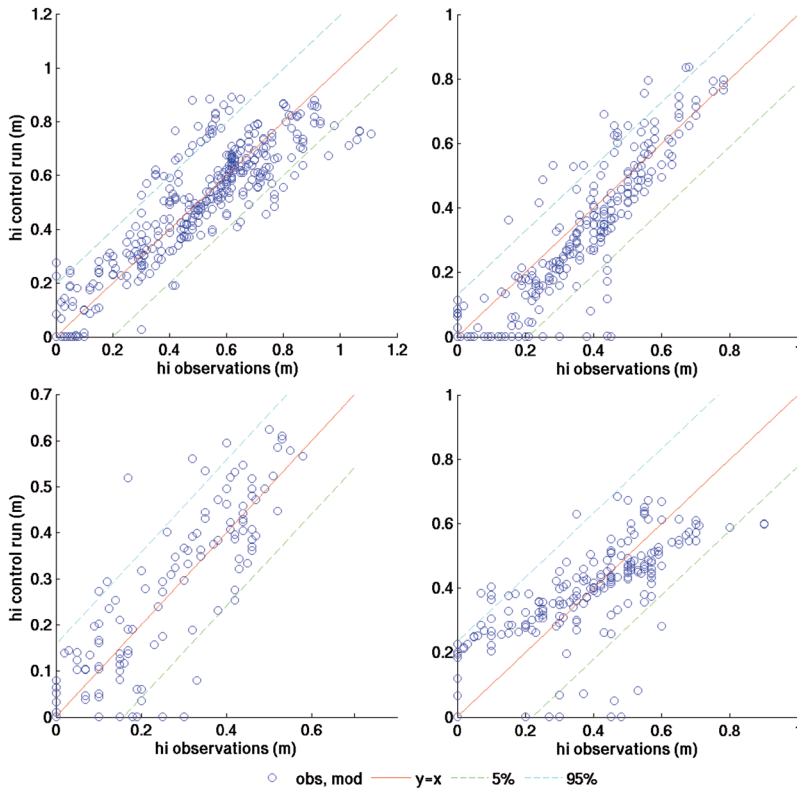


Fig. 4. Observations and model simulations at Jussarö (above) and Kotka (below) stations for 1979–1993. The two types of snow are grouped together ( $h_s$ ) and plotted in the positive ordinate. Snow ice and superimposed ice are also grouped together as an intermediate layer ( $h_m$ ) and plotted in the negative ordinate. The total ice thickness ( $h_{i\text{ tot}}$ ) is shown in the negative ordinate as the sum of the intermediate layer and the sea-ice thickness.

heat fluxes (*see* the following section on model calibration and sensitivity). The model seems to reproduce the dominant physical features well (*see* Figs. 3 and 4): timing of growth/melting

and thickness of the ice layers are generally in good agreement with observations at all stations, except for few cases — for example in Ajos, Jussarö and Kotka during the ice season 1985–1986.



**Fig. 5.** Observations of ice thickness plotted against control simulations at Ajos, Kummelgrund, Jussarö and Kotka (from above, clockwise). The ice thickness is plotted on the x-axis against the model control run in the y-axis. The red line is the perfect fit with observations, while the dashed blue and green lines represent the 5% and 95% confidence intervals of every distributions of residuals (difference between observed ice thickness and modelled ice thickness), which are assumed to be normal.

Nonetheless, the model generally underestimated the maximum thickness of the snow layer, especially in Ajos — for example during the ice seasons 1980/1981 and 1987/1988. This is probably due to the fact that snow compaction is initiated when new precipitation falls on old snow. However, since the total weight of snow on ice is conserved, the mismatch between simulations and observations do not affect the total ice thickness (Fig. 5).

The statistical analysis (Table 2) of the residuals reveals low variance values, ranging between 0.93 and 1.89 cm. The linear correlation coef-

ficient is high, from 0.7375 in Kotka to 0.9012 in Kummelgrund. The root-mean-square errors remain low, between 9.65 and 11.14 cm. The kurtosis index is, instead, always greater than 3, showing that all of the distributions are more outlier-prone than a normal distribution is. Also the skewness index reveals that 3 out of 4 of the residuals distributions spread out more to the left, while only the Ajos residual distributions spreads out slightly to the right.

Most of the mismatches between observations and model runs are generally greater at the beginning and/or at the end of the ice season (*see*

**Table 2.** Statistics of ice thickness residuals for the control simulations.

Site	Calibration parameters		Ice thickness residuals (m) (observation/model results)					
	Albedo	$F_w$ ( $W\ m^{-2}$ )	Mean	Variance	Correlation	RMSE	Kurtosis	Skewness
Ajos	FB96	6	-0.0010	0.01440	0.8812	0.1114	3.9337	0.2407
Kummelgrund	FB96	0	-0.0393	0.0105	0.9012	0.1022	5.4249	-0.2206
Jussarö	FB96	7	-0.0002	0.0093	0.8738	0.0965	4.9824	-0.4331
Kotka	FB96	9	0.0061	0.0189	0.7375	0.1109	4.3011	-0.6862

Fig. 5). The largest discrepancy is in Kummelgrund, where, despite the fact that the oceanic heat flux is set to  $0 \text{ W m}^{-2}$ , the mean residual value is  $-3.93 \text{ cm}$ , indicating a general underestimation of the modelled total ice thickness.

## Model calibration and sensitivity

In model developments, the choice of the tuning parameters to adjust the model results is usually guided by considering their uncertainties and sensitivities, choosing justifiable values, minimizing the number of parameters, whose values must be changed once a time. The model has been initially calibrated by testing several albedo parameterizations and oceanic heat fluxes and analysed by means of the model sensitivity to their values.

Sea ice is known to be very sensitive to albedo (Shine and Henderson-Sellers 1985), which is the ratio of the reflected and absorbed radiation. The higher the albedo is, the smaller the absorbed heat and larger the reflected radiation are. Surface albedo is dependent on the surface type (snow or ice), surface temperature and the age of the surface layer. In order to calibrate our model, we tested the discrete parameterization of the albedo developed by Perovich *et al.* (1996, hereafter referred to as PE96) for the central Arctic and the continue algorithms developed by Flato and Brown (1996, hereafter referred to as FB96) for the Arctic landfast sea ice and by Pirazzini *et al.* (2006, hereafter referred to as PI06) for the Baltic landfast sea ice.

Sea ice also receives a certain amount of heat from the ocean underneath, which is a function of the sea water temperature and contributes to the melting of sea ice from the bottom. In our model system, the slab ocean only computes the sea water temperature when the surface is ice/snow-free. Otherwise the sea water temperature is fixed at the freezing point of seawater and the ocean heat flux constant. When the oceanic heat flux is large or highly variable, a proper determination of  $F_w$  may necessitate of a fully-coupled sea-ice-ocean model (e.g. Maykut and McPhee 1995). However, in marginal seas the stratification beneath the ice tends to be stable and  $F_w$  remains small or not very variable. Thus the oceanic heat flux may be considered constant (Launiainen and Cheng 1998). The Baltic Sea is an extreme example, being permanently stratified throughout the year and the heat contribution from below very limited.

First, we ran ESIM1 using the three different parameterizations of the albedo (PE96, FB96 and PI06) and 4 different oceanic heat-flux values ( $0, 3, 6, 9 \text{ W m}^{-2}$ ). As a result, we produced 12 simulations for every station. Total ice thickness was chosen as a target variable for the model calibration and we analysed the residuals, that is the difference between the observed ice thickness and the model ice thickness. We computed the mean, variance, kurtosis and skewness indices of the residuals for every simulation. Finally, we chose to use the albedo parameterization and the oceanic heat-flux value that produced the best statistical results and the best fit of the residuals (Table 2).

**Table 3.** Ice thickness residuals for model calibration to albedo.

Parameterization	Site	$F_w$ ( $\text{W m}^{-2}$ )	Mean (m)	Variance (m)	Kurtosis index	Skewness index
PE96	Ajos	6	0.0046	0.0163	4.3264	0.5273
	Kummelgrund	0	-0.0238	0.0159	8.4157	1.3988
	Jussarö	7	0.0396	0.0091	4.9674	0.6154
	Kotka	9	0.0245	0.0241	4.9458	-0.7115
FB96	Ajos	6	-0.0010	0.0144	3.9337	0.2407
	Kummelgrund	0	-0.0393	0.0105	5.4249	-0.2206
	Jussarö	7	-0.0002	0.0093	4.9824	-0.4331
	Kotka	9	0.0061	0.0189	4.3011	-0.6862
PI06	Ajos	6	0.0037	0.0152	4.2283	0.4555
	Kummelgrund	0	-0.0315	0.0126	6.7599	0.5772
	Jussarö	7	0.0195	0.0081	5.0251	0.4473
	Kotka	9	0.0227	0.0194	4.4513	-0.6770

At every station, the albedo parameterization of FB96 showed to produce the best results (Table 3), followed by PI06 and PE96, whose parameterizations, instead, tended to slightly overestimate the total ice thickness. Looking forward to more general applications and couplings of ESIM in the future and also to the fact that the FB96 parameterization reduced the numbers of albedo parameters from 7 to 5 as compared with the one of PE96, we agreed the FB96 parameterization as the best one for landfast sea ice. About the oceanic heat-flux, we chose those values to get the best-fit simulations, ranging from 0 W m<sup>-2</sup> at Kummelgrund to 6 W m<sup>-2</sup> at Ajos, to 7 W m<sup>-2</sup> at Jussarö and at 9 W m<sup>-2</sup> in Kotka (Tables 2 and 3).

In order to understand the sensitivity of ESIM1 to the choice of the albedo parameterization of FB96 and to the value of the oceanic fluxes we assumed, we performed a sensitivity analysis by using the *S* index (Eq. 8) for one of the test-case station (Ajos).

The assumed value of the oceanic heat-flux ( $F_w$ ) at Ajos is 6 W m<sup>-2</sup>. We thus ran the model also with  $F_w = 5.4$  W m<sup>-2</sup> (-10%) and  $F_w = 6.6$  W m<sup>-2</sup> (+10%). The *S* index was 0.5460, which is a high value.

The FB96 albedo parameterization assumes two different snow albedos in freezing (“winter”) and non-freezing (“summer”) conditions, while the sea-ice albedo depends on the snow and sea-ice thickness. Since the FB96 algorithm does not include any parameterization of the snow-ice and superimposed-ice albedos, we used those formulated by Perovich (1996) for compacted snow and melting white ice. At each of those albedos we added and subtracted 10% of their values for totally 12 simulations at Ajos (for *S* see Table

4). Even the highest sensitivity of the model to the snow “winter” albedo is very small (0.0994), showing that ESIM1 is very robust to small variations of albedo ( $\pm 10\%$ ) in our simulations.

## Sensitivity to physical processes

ESIM1 is a very comprehensive sea-ice thermodynamic model, in terms of the number of physical processes included. We analysed the sensitivity of ESIM1 to coupling with a simple ocean mixed-layer and to the superimposed-ice and snow-ice formations.

We changed ESIM1 similarly to a simple Semtner 0-layer sea-ice model (hereafter referred to as SIMPLE1), that is with only one layer of sea ice and one layer of snow on top of it, without considering any snow metamorphism. SIMPLE1 overestimated the snow thickness by about 27 cm and, consequently, the ice thickness was underestimated by about 17 cm (Fig. 6a).

In SIMPLE2 (Fig. 6b), we added to SIMPLE1 a simple ocean mixed-layer 10-m-thick underneath sea-ice. Comparing SIMPLE2 with SIMPLE1 we obtained a slightly better estimation of snow thickness (23.60 cm overestimation) and ice thickness (16.28 cm underestimation). The inclusion of a slab ocean underneath the sea ice produced a better agreement with the date of freezing/melting. Thus we kept the coupled configuration with the slab ocean in all the other simulations.

SIMPLE3 also included the superimposed-ice formation process (Eqs. 4 and 5). The snow overestimation slightly decreased to 23.10 cm, while the ice underestimation decreased to 14.51 cm. Therefore, superimposed ice shows to give a rather small contribution, in terms of thickness, to the total ice mass balance (Fig. 6c).

In the last case, SIMPLE4, snow-ice formation (Eq. 6) was added to SIMPLE2 and we plotted simulation results of ESIM1 together with SIMPLE4 (Fig. 6d). The role and the contribution of the snow ice to the total ice mass is very evident. The discrepancy between ESIM1 and SIMPLE4 snow thickness is reduced to 0.42 cm, while the difference between ESIM1 and SIMPLE4 ice thickness is now 0.22 cm.

**Table 4.** Model sensitivity to albedo (Ajos).

Albedo	<i>S</i>
Winter snow	0.0994
Winter meteoric ice	0.0193
Winter sea ice	0.0024
Summer snow	0.0788
Summer meteoric ice	0.0529
Summer sea ice	0.0500

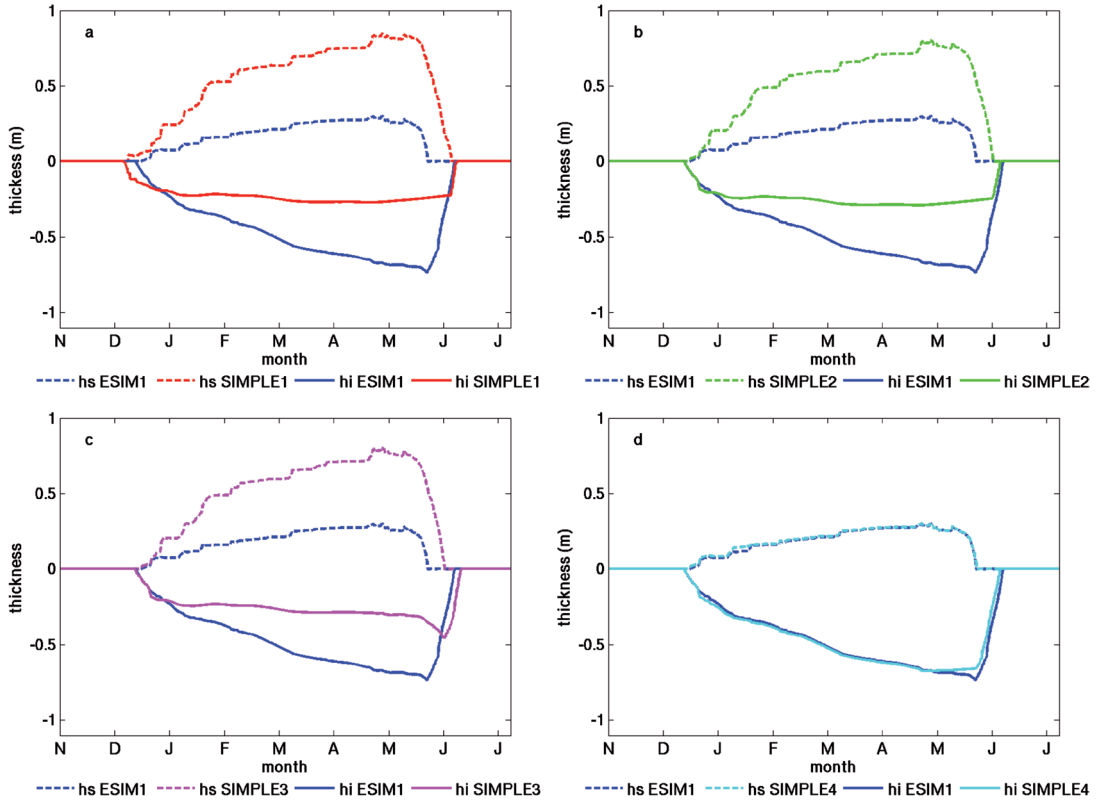


**Fig. 6.** Comparisons among ESIM1 and SIMPLE. (a) ESIM1 vs. SIMPLE1 (no slab ocean, no meteoric ice). (b) ESIM1 vs. SIMPLE2 (with slab ocean). (c) ESIM1 vs. SIMPLE3 (with slab ocean and superimposed ice). (d) ESIM1 vs. SIMPLE4 (with slab ocean and snow ice).

## Scenario analyses for atmospheric forcing

The model was forced by the ECMWF ERA-15 and NCEP 6h Reanalysis data at 2.5 degrees resolution. The choice of such a coarse resolution database was driven by the plans of using this model also in coupled configurations within ESMs.

In order to assess the robustness of the model to the forcing data we used, we performed a scenario analysis for one of the test-case site (Ajos). We added/removed 10% of the value of each forcing at every time step, one-by-one for all the 7 meteorological data. Totally, we produced 14 “perturbed” simulations to be compared with the control simulation and with the observations of total ice thickness. We analysed the model results by means of a Taylor Diagram: a way of

graphically summarizing how closely a pattern (or set of pattern) matches observations (Taylor 2001). The similarity between patterns is quantified in terms of their correlation, their centered-root-mean-square difference and the amplitude of their variations (represented by standard deviations).

All of the simulations have a relative high correlation with observations (0.87–0.89) and their root-mean-square errors remain constant between 0.11 and 0.12 m. The only slight difference among simulations is their standard deviation, which ranges from 0.22 to 0.25 m, but it always remains smaller than the standard deviation of the observations (slightly higher than 0.25 m) (Fig. 7). Consequently, there is no significant difference among the control and the perturbed simulations.

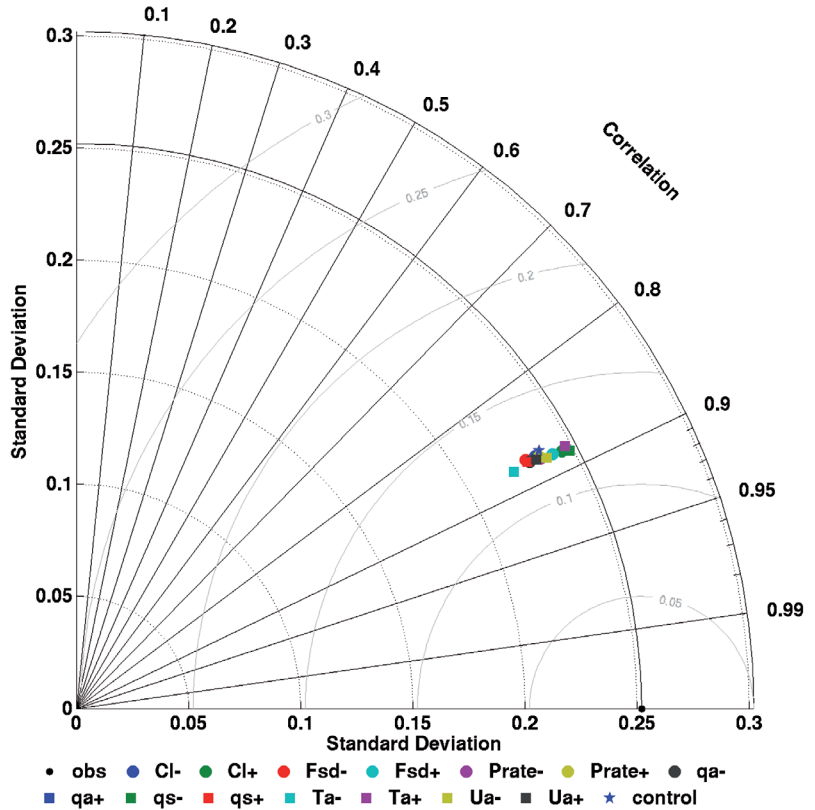


**Fig. 7.** Taylor diagram presenting standard deviations, root mean square errors and correlations for the ice thickness observations (black dot), control simulation (blue star) and 14 perturbed simulations (CI: total cloud cover, Fsd: irradiance, Prate: precipitation rate, qa: specific humidity at 2 m height, qs: specific humidity at the surface, Ta: air temperature at 2 m height, Ua: wind speed at 10 m height) at Ajos.

## Discussion and conclusions

In order to properly simulate an ice season, it is necessary to include in any sea-ice model the important physical processes responsible of the sea-ice/snow accumulation, growth, metamorphism and decay.

In other regions of the globe, ice thickness may be greater (Arctic and Antarctic multi-year ice), the amount of precipitation smaller (especially in the Arctic) and consequently the snow-ice formation may play a minor role. In the Baltic Sea (i.e. Granskog *et al.* 2004) — but also in large areas of the Antarctic (i.e. Ross Sea, Kawamura *et al.* 2004) — snow-ice plays a very important physical and biological roles and gives a relevant contribution — up to 50% (Kawamura *et al.* 2001) — to the total ice mass balance (SIMPLE4). Besides, the Baltic Sea is characterized by rather more complex melt-freeze cycles, mainly due to its mild and wet climate, which leads to the inclusion of superimposed

ice (SIMPLE3), which is usually neglected in sea-ice models. Moreover, the superimposed-ice growth is peculiar of the Baltic Sea (Granskog *et al.* 2003) and the lowest Arctic (e.g. Svalbard area, Nicolaus *et al.* 2003).

The sensitivity test of the physical processes shows that the ESIM1 does a good job whenever the snow layer is well simulated and it is not necessary to add more sea-ice layers to better reproduce the total ice thickness. The model is, instead, very sensitive to the meteoric ice dynamics and snow is the key variable in sea-ice modelling because of its different metamorphoses, high albedo and strong insulating effect. We suggest that more attention should be paid to snow accumulation, compaction and metamorphoses to further improve our results. Even though the meteoric-ice formation is especially relevant for the Baltic sea-ice and for Antarctic first-year ice, in a climate change scenario of thinning of the ice and increasing of precipitation, (i.e. Alexander *et al.* 2004), snow ice and superimposed ice

may become more common and important in the Arctic and the Antarctic as well.

The calibration and the related sensitivity test to some model parameters stresses the relevant role of the oceanic heat flux in sea-ice modelling. The oceanic heat flux, especially when it is assumed to be constant, is a continuous source of heat from the ocean to sea ice and has a relevant role in the heat budget at the bottom of the ice sheet. Consequently, it has a strong effect on the resulting total ice thickness and this has to be taken into account when a sea-ice model is running in coupled configurations and when is the ocean to compute the seawater temperature. However, the model does not seem to be very sensitive to small variations of the surface albedo. Even the highest sensitivity value for winter snow albedo is rather small, showing that ESIM1 is very robust to small changes in this important parameter for our test-case sites. Further applications will show if ESIM1 is robust enough for the entire coastal Baltic Sea and for other coastal ice-covered oceans.

Coupled models and particularly ESMs generally have resolutions comparable or slightly finer than those of the reanalysis data used here. From the scenarios analysis, we found that the perturbed model simulations do not significantly differ from the control run and we can then conclude that such coarse resolution of the forcing data can be acceptable for long-term simulations of sea-ice thermodynamics.

In this paper, we presented ESIM1, an enhanced and comprehensive — in terms of the number of physical processes included — sea-ice thermodynamic model, developed and applied to the landfast sea ice. ESIM1 reasonably reproduces the inter-annual variability of the sea-ice season in the ice-covered Baltic Sea. Some of the main physical features of the sea-ice and snow evolution are rather well reproduced. Particularly, the thickness of the ice layers and the timing of growing/melting are generally in good agreement with observations. This new structure, which stresses the importance of the snow/ice metamorphism rather than the number of sea-ice layers, makes Semtner-like models more comprehensive and, at the same time, reduces the computational requirements, making the model

more suitable for coupled configurations with other physical models.

Model results are sufficiently robust for an appropriate simulation of the ice characteristics functional to the Baltic Sea biota, where sea-ice salinity plays a minor role, being close to 0‰, and usually characterized by constant in time vertical profile. Further improvements, which will make the model more suitable for application in other polar and subpolar regions, concern the inclusion of a halodynamic component in ESIM1. ESIM2 will then be coupled to an improved version of the Biogeochemical Flux Model (BFM, Vichi *et al.* 2007a, 2007b).

*Acknowledgements:* This study is supported by the VECTOR project, funded by the Italian Ministry of the University and the Scientific Research. Collaboration with the Finnish Institute of Marine Research has started thanks to the “Marco Polo” scholarship awarded by the University of Bologna to the first author. NCEP Reanalysis and ECMWF data have been provided by the NOAA/OAR/ESRL PSD, Boulder, Colorado, USA, from their Web site at <http://www.cdc.noaa.gov/>. The observed snow and ice thickness data have been provided by the Ice Service at the Finnish Institute of Marine Research. We are particularly grateful to Ari Seinä for support with the observations. We acknowledge the support from the Eur-Oceans network of excellence funded under the EU FP6 — Global change and ecosystems, Contract number 511106.

## References

- Alexander M.A., Bhatt U.S., Walsh J., Timlin M.S., Miller J.S. & Scott J.D. 2004. The atmospheric response to realistic Arctic sea ice anomalies in a AGCM during winter. *J. Climate* 17: 890–905.
- Cheng B., Vihma T., Pirazzini R. & Granskog M.A. 2006. Modelling of superimposed ice formation during the spring snowmelt period in the Baltic Sea. *Ann. Glaciol.* 44: 139–146.
- Cox G.F.N. & Weeks W.F. 1988. Numerical simulations of the profile properties of undeformed first-year sea ice during the growth season. *J. Geoph. Res.* 93(C10): 12444–12460.
- Eicken H. 2003. From the microscopic, to the macroscopic, to the regional scale: growth, microstructure and properties of sea ice. In: Thomas D.N. & Dieckmann G.S. (eds.), *Sea ice: an introduction to its physics, biology, chemistry and geology*, Blackwell Science, Oxford, pp. 22–81.
- Fichefet T. & Morales Maqueda M.A. 1999. Modelling the influence of snow accumulation and snow-ice formation on the seasonal cycle of the Antarctic sea-ice cover. *Climate Dynamics* 15: 251–268.

- Flato G.M. & Brown R.D. 1996. Variability and climate sensitivity of landfast Arctic sea ice. *J. Geophys. Res.* 101(C10): 25 767–25 778.
- Gibson J.K., Kallberg P., Uppala S., Nourmura A., Hernandez A. & Serrano E. 1997. *ERA description*. ECMWF Re-Analysis Project Report Series 1, ECMWF, Reading, UK.
- Granskog M.A., Martma T.A. & Vaikmäe R.A. 2003. Development, structure and composition of land-fast sea ice in the northern Baltic Sea. *J. Glaciol.* 49: 139–148.
- Granskog M.A., Leppäranta M., Kawamura T., Ehn J. & Shirasawa K. 2004. Seasonal development of the properties and composition of landfast sea ice in the Gulf of Finland, the Baltic Sea. *J. Geophys. Res.* 109(C2): C02020, doi: 10.1029/2003JC001874.
- Kalnay E., Kanamitsu M., Kistler R., Collins W., Deaven D., Gandin L., Iredell M., Saha S., White G., Woollen J., Zhu Y., Leetmaa A., Reynolds B., Chelliah M., Ebisuzaki W., Higgins W., Janowiak J., Mo K., Ropelewski C., Wang J., Jenne R. & Joseph D. 1996. The NCEP/NCAR 40-year reanalysis project. *Bull. Amer. Meteor. Soc.* 77: 437–471.
- Kawamura T., Shirasawa K., Ishikawa N., Lindfors A., Rasmus K., Granskog M.A., Ehn J., Leppäranta M., Martma T. & Vaikmäe R. 2001. Time-series observations of the structure and properties of brackish ice in the Gulf of Finland. *Ann. Glaciol.* 33: 1–4.
- Kawamura T., Jeffries M.O., Tison J.L. & Krouse H.R. 2004. Superimposed ice formation in summer on Ross Sea pack ice floes. *Ann. Glaciol.* 39: 56–568.
- Launiainen J. & Cheng B. 1998. Modelling of ice thermodynamics in natural water bodies. *Cold Regions Science and Technology* 27: 153–178.
- Leppäranta M. 1983. A growth model for black ice, snow-ice and snow thickness in subarctic basins. *Nordic Hydrol.* 14: 59–70.
- Maykut G.A. & Untersteiner N. 1971. Some results from a time dependent thermodynamic model of sea-ice. *J. Geophys. Res.* 76: 1550–1575.
- Maykut G.A. & McPhee M.G. 1995. Solar heating of the Arctic mixed layer *J. Geophys. Res.* 100(C12): 24691–25703.
- Nicolaus M., Haas C. & Bareiss J. 2003. Observations of superimposed ice formation at melt-onset on fast ice on Kongsfjorden, Svalbard. *Phys. Chem. Earth* 28: 1241–1248.
- Perovich D.K. 1996. The optical properties of sea ice. *CREEL monograph* 96-1: 1–25.
- Pirazzini R., Vihma T., Granskog M.A. & Cheng B. 2006. Surface albedo measurements over sea ice in the Baltic Sea during the spring snowmelt period. *Ann. Glaciol.* 44: 7–14.
- Saltelli A. 2005. Global sensitivity analysis: an introduction. In: Hanson K.M. & Hemez F.M. (eds.), *Sensitivity analysis of model output*, Los Alamos National Laboratory, available at <http://library.lanl.gov/cgi-bin/getdoc?event=SAMO2004&document=samo04-08.pdf>.
- Schmidt G.A., Bitz C., Mikolajewicz U. & Tremblay L.-B. 2004. Ice-ocean boundary conditions for coupled models. *Ocean Modelling* 7: 59–74.
- Semtner A.J. 1976. A model for the thermodynamic growth of sea ice in numerical investigation of climate. *J. Phys. Oceanogr.* 6: 379–389.
- Shine K.P. & Hederson-Sellers A. 1985. The sensitivity of a thermodynamic sea ice model to changes in surface albedo parametrizations. *J. Geophys. Res.* 90: 2243–2250.
- Stefan J. 1891. Über die Theorie der Eisbildung, insbesondere über Eisbildung im Polarmeere. *Ann. Phys.* 42: 269–286.
- Taylor K.E. 2001. Summarizing multiple aspects of model performance in a single diagram. *J. Geophys. Res.* 106: 7183–7192.
- Untersteiner N. 1964. Calculations of temperature regime and heat budget of sea-ice in the central Arctic. *J. Geophys. Res.* 69: 4755–4766.
- Vichi M., Pinardi N. & Masina S. 2007a. A generalized model of pelagic biogeochemistry for the global ocean ecosystem. Part I: Theory. *J. Mar. Sys.* 64: 89–109.
- Vichi M., Masina S. & Navarra A. 2007b. A generalized model of pelagic biogeochemistry for the global ocean ecosystem. Part II: Numerical simulations. *J. Mar. Sys.* 64: 110–134.